

Inferring networks from time series: a neural approach

Thomas Gaskin^[1,2,*]

Grigorios A. Pavliotis^[2]

Mark Girolami^[3,4]

¹Department of Applied Mathematics and Theoretical Physics, University of Cambridge, Cambridge CB3 0WA, United Kingdom;

²Department of Mathematics, Imperial College London, London SW7 2AZ, United Kingdom; ³Department of Engineering, University of Cambridge, Cambridge CB2 1PZ, United Kingdom; ⁴The Alan Turing Institute, London NW1 2DB, United Kingdom

*To whom correspondence should be addressed: trg34@cam.ac.uk

Abstract

Network structures underlie the dynamics of many complex phenomena, from gene regulation and foodwebs to power grids and social media. Yet, as they often cannot be observed directly, their connectivities must be inferred from observations of their emergent dynamics. In this work we present a powerful computational method to infer large network adjacency matrices from time series data using a neural network, in order to provide uncertainty quantification on the prediction in a manner that reflects both the non-convexity of the inference problem as well as the noise on the data. This is useful since network inference problems are typically underdetermined, and a feature that has hitherto been lacking from such methods. We demonstrate our method's capabilities by inferring line failure locations in the British power grid from its response to a power cut. Since the problem is underdetermined, many classical statistical tools (e.g. regression) will not be straightforwardly applicable. Our method, in contrast, provides probability densities on each edge, allowing the use of hypothesis testing to make meaningful probabilistic statements about the location of the power cut. We also demonstrate our method's ability to learn an entire cost matrix for a non-linear model of economic activity in Greater London. Our method outperforms OLS regression on noisy data in terms of both speed and prediction accuracy, and scales as N^2 where OLS is cubic. Not having been specifically engineered for network inference, our method represents a general parameter estimation scheme that is applicable to any parameter dimension.

Keywords: Network inference, Neural differential equations, Model calibration, Power grids.

Contents

| | | | |
|--|---|---|----|
| I Introduction | 2 | IV Performance analysis and comparison with OLS | 9 |
| II Inferring line failures in the British power grid | 3 | V Quantifying uncertainty | 10 |
| III Inferring economic cost networks from noisy data | 7 | VI Discussion | 11 |
| | | Supporting Information | 15 |

I. Introduction

Networks are important objects of study across the scientific disciplines. They materialise as physical connections in the natural world, for instance as the mycorrhizal connections between fungi and root networks that transport nutrients and warning signals between plants [1, 2], human traffic networks [3, 4], or electricity grids [5, 6]. However, they also appear as abstract, non-physical entities, such as when describing biological interaction networks and food webs [7–9], gene or protein networks [10, 11], economic cost relations [12, 13], or social links between people along which information (and misinformation) can flow [14–16]. In all examples, though the links constituting the network may not be tangible, the mathematical description is the same. In this work, we are concerned with inferring the structure of a network from observations of its dynamics. The problem is of great scientific bearing: for instance, one may wish to understand the topology of an online social network from observing how information is passed through it, and some work has been done on this question [17–19]. Another important application is inferring the connectivity of neurons in the brain by observing their responses to external stimuli [20, 21]. In an entirely different setting, networks crop up in statistics in the form of conditional independence graphs, describing dependencies between different variables, which again are to be inferred from data [22, 23].

Our approach allows inferring network connectivities from time series data with uncertainty quantification. Uncertainty quantification for network inference is important for two reasons: first, the observations will often be noisy, and one would like the uncertainty on the data to translate to an uncertainty on the predicted network. Secondly however, completely inferring large networks requires equally large amounts of data – typically at least $N - 1$ equations per node, N being the number of nodes – and these observations must furthermore be linearly independent. Data of such quality and quantity will often not be available, leading to an under-determined inference problem. The uncertainty on the

predicted network should thus also reflect (at least to a certain degree) the non-convexity of the problem under consideration: how many networks are compatible with the observed data? To the best of our knowledge, no current network inference method is able to provide this information.

Network inference can be performed using ordinary least squares (OLS) regression [6, 24], but this is confined to the case where the dynamics are linear in the adjacency matrix. In addition, without additional constraints OLS usually only works when the network is uniquely identifiable, and its computational cost typically scales as N^3 , making it infeasible for larger networks. Our method avoids these limitations. Computationally fast network inference methods have been developed [17–19], but these tend to be highly specialised to a particular type of observation data and give no uncertainty quantification on the network prediction. Our method, by contrast, is versatile, not having been specifically engineered to fit the network case, and having previously been applied to learn low-dimensional vectors of parameters for stochastic differential equations [25]. The presented approach is thus not limited to networks, but constitutes a general parameter estimation method.

Method description We apply the method proposed in [25] to the network case. The approach consists of training a neural network to find a graph adjacency matrix $\hat{\mathbf{A}} \in \mathbb{R}^{N \times N}$ that, when inserted into the model equations, reproduces a given time series $\mathbf{T} = (\mathbf{x}_1, \dots, \mathbf{x}_L)$. A neural network is a function $u_\theta : \mathbb{R}^{N \times q} \rightarrow \mathbb{R}^p$, where $q \geq 1$ represents the number of time series steps that are passed as input. Its output is the (vectorised) estimated adjacency matrix $\hat{\mathbf{A}}$, which is used to run a numerical solver for B iterations (B is the batch size) to produce an estimated time series $\hat{\mathbf{T}}(\hat{\mathbf{A}}) = (\hat{\mathbf{x}}_1, \dots, \hat{\mathbf{x}}_{i+B})$. This in turn is used to train the internal parameters θ of the neural net (the weights and biases) via a loss function $J(\hat{\mathbf{T}}, \mathbf{T})$. As $\hat{\mathbf{A}} = \hat{\mathbf{A}}(\theta)$, we may calculate the gradient $\nabla_\theta J$ and use it to optimise the internal parameters of the neural net using a backpropagation method of choice; popular choices include stochastic gradient descent, Nesterov schemes, or the Adam optimizer [26]. Calculating $\nabla_\theta J$ thus requires differentiating the predicted time series $\hat{\mathbf{T}}$, and thereby the system equations, with respect to $\hat{\mathbf{A}}$. In other words: the loss function

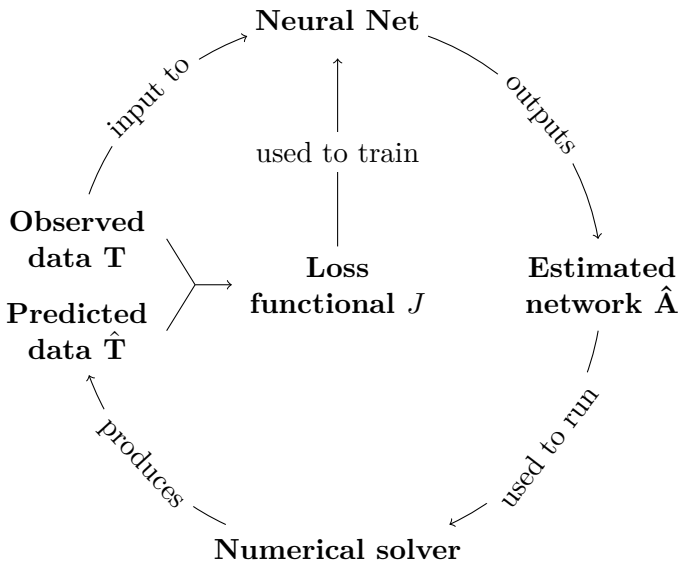


Figure 1: The methodological pipeline from [25] used in this work. The neural net u_θ takes q time series elements as input and outputs a predicted network adjacency matrix. These predictions are fed into a numerical solver, which produces a predicted time series. The true and predicted time series are used to generate a loss functional, which in turn can be used to train the neural net’s internal parameters θ . The goal is to retrieve the true network \mathbf{A} from the data. A single pass over the entire dataset is called an *epoch*. The dataset is processed in *batches*, meaning the loss is calculated over B steps of the time series before the weights are updated. If $B = L$, training is equivalent to batch gradient descent; if $B = 1$, training is equivalent to stochastic gradient descent.

contains knowledge of the dynamics of the model. Finally, the true data is once again input to the neural net to produce a new parameter estimate $\hat{\mathbf{A}}$, and the cycle starts afresh. A single pass over the entire dataset is called an epoch; see fig. 1.

Using a neural net allows us to exploit the fact that, as the net trains, it traverses the space of all graphs, calculating a loss at each point. By tracking its path and gathering the loss values we are able to construct a probability density on the adjacency matrix, allowing for uncertainty quantification. The method is in effect a Gibbs sampling scheme [27], where we wish to obtain the joint distribution

$$p(\hat{\mathbf{A}}, \hat{\mathbf{T}} \mid \mathbf{T}) = \int p(\hat{\mathbf{A}}, \hat{\mathbf{T}}, \theta \mid \mathbf{T}) d\theta$$

by marginalising over the training steps. We sample

from this joint density by cyclically sampling from the estimated network $\hat{\mathbf{A}}$, the estimated data $\hat{\mathbf{T}}$, and the neural network weights and biases θ from conditional densities and using each sample for the next conditional:

$$\hat{\mathbf{A}}^{i+1} \sim p(\hat{\mathbf{A}} \mid \hat{\mathbf{T}}^i, \theta^i, \mathbf{T}) \quad (1)$$

$$\hat{\mathbf{T}}^{i+1} \sim p(\hat{\mathbf{T}} \mid \hat{\mathbf{A}}^{i+1}, \theta^i, \mathbf{T}) \quad (2)$$

$$\theta^{i+1} \sim p(\theta \mid \hat{\mathbf{A}}^{i+1}, \hat{\mathbf{T}}^{i+1}, \mathbf{T}). \quad (3)$$

Here, i is the training iteration index. Each of the three densities represents different components in the cycle: eq. [1] is the neural net’s output, which is deterministic:

$$\hat{\mathbf{A}}^{i+1} = u_{\theta^i}(\hat{\mathbf{T}}^i).$$

Eq. [2] is the output of the numerical solver, which may be stochastic, depending on whether the numerical solver is run with noise:

$$p(\hat{\mathbf{T}} \mid \hat{\mathbf{A}}^{i+1}, \theta^i, \mathbf{T}) \sim \rho_{NS}(\hat{\mathbf{A}}^{i+1}).$$

Finally, the updated neural network parameters eq. [3] are drawn using the gradient descent scheme.

By Bayes’ rule,

$$p(\hat{\mathbf{A}}, \hat{\mathbf{T}}, \theta \mid \mathbf{T}) \sim \exp(-\|\hat{\mathbf{T}} - \mathbf{T}\|_2) \pi^0(\hat{\mathbf{A}}) \pi^0(\theta) \pi^0(\hat{\mathbf{T}}),$$

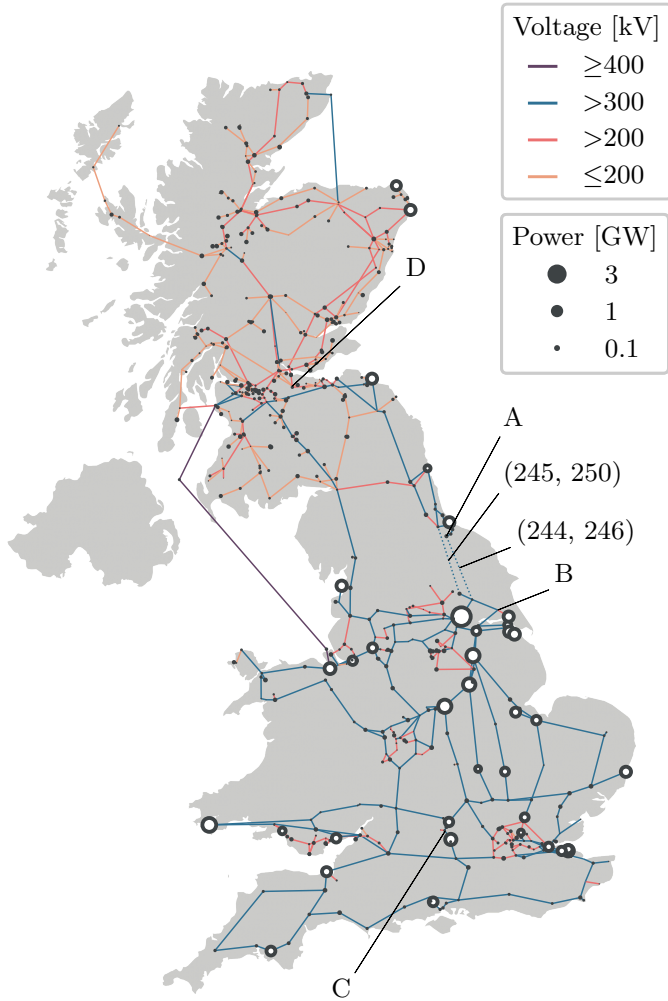
with π^0 the priors, and $\exp(-\|\hat{\mathbf{T}} - \mathbf{T}\|_2)$ the likelihood function [28].

We begin this article with two application studies: first, we infer locations of a power line cut in the British power grid from observations of the network response to the cut; and secondly, we infer economic cost relations between retail centres in Greater London. Thereafter we conduct a comparative analysis of our method’s performance, before finally analysing the relationship between uncertainty in the data, the convexity of the problem, and the prediction uncertainty.

II. Inferring line failures in the British power grid

Power grids can be modelled as networks of coupled oscillators using the Kuramoto model [33–37]. Each node i in the network either produces or consumes electrical power P_i while oscillating at the grid reference frequency Ω . The nodes are connected through a weighted

(a) Power grid topology



(b) Network response to line failure

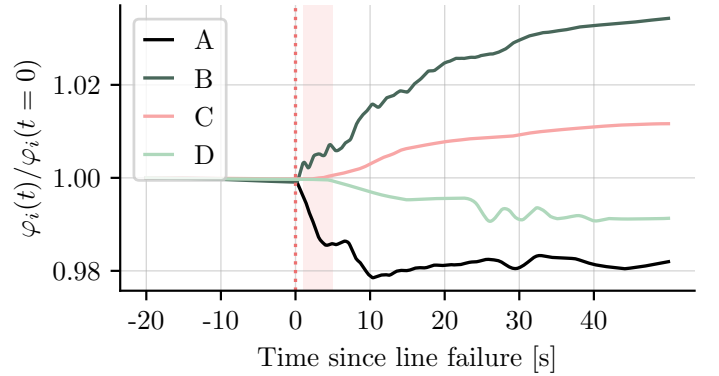


Figure 2: (a) Approximate high-voltage electricity transmission grid of Great Britain. Shown are 630 accurately placed nodes, representing power stations, substations, and transmission line intersections, and their connectivity as of January 2023 [29–31]. Colours indicate the operating voltage of the lines. The size of the nodes indicate their power generation or consumption capacity (absolute values shown). White ringed nodes indicate the 38 nodes that are real power stations with capacities over 400 MW [32], with all other nodes assigned a random capacity in $[-200, +200]$. The two dotted edges in the northeast of England are the edges affected by a simulated power cut, labelled by the indices of their start and end vertices. (b) The network response to the simulated power line failure, measured at four different nodes in the network (marked A–D). The equation parameters were tuned to ensure phase-locking of the oscillators ($\alpha = 1$, $\beta = 0.2$, $\kappa = 30$). Nodes closer to the location of the line cut (A and B) show a stronger and more immediate response than nodes further away (C and D). The shaded area indicates the 4-second window we use to infer the line location.

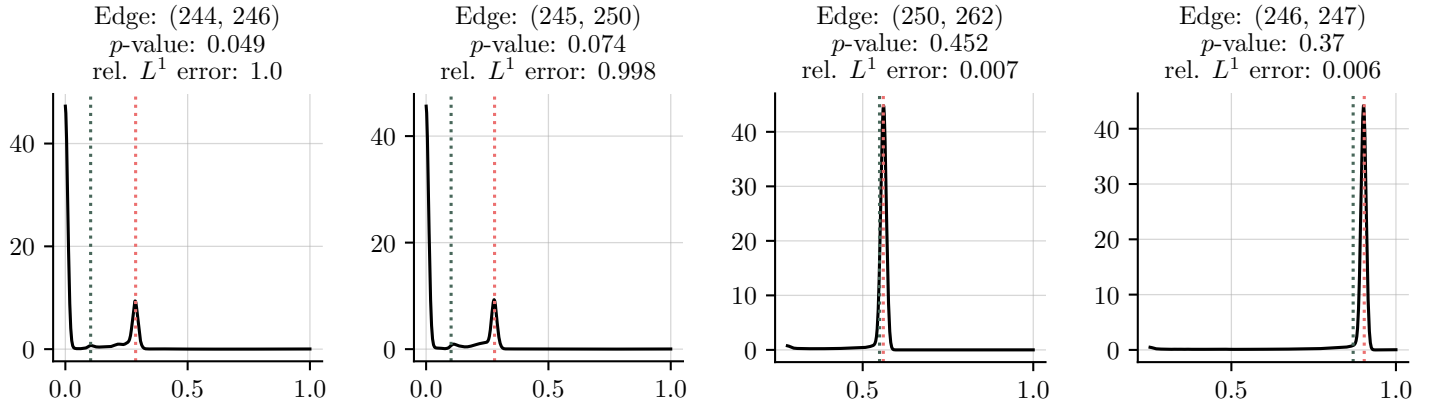
undirected network $\mathbf{A} = (a_{ij})$, where the link weights $a_{ij} \sim Y_{ij}U_{ij}^2$ are obtained from the electrical admittances Y_{ij} and the voltages U_{ij} of the lines. The network coupling allows the phases $\varphi_i(t)$ of the nodes to synchronise according to the differential equation [36]

$$\alpha \frac{d^2 \varphi_i}{dt^2} + \beta \frac{d\varphi_i}{dt} = P_i + \kappa \sum_j a_{ij} \sin(\varphi_j - \varphi_i), \quad (4)$$

where α , β , and κ are the inertia, friction, and coupling coefficients respectively. A requirement for dynamical stability of the grid is that $\sum_i P_i = 0$, i.e. that as much power is put into the grid as is taken out through consumption and energy dissipation [35].

A power line failure causes the network to redistribute the power loads, causing an adjustment cascade to ripple through the network until equilibrium is restored [5]. In this work we recover the location of a line failure in the British power grid from observing these response dynamics. Figure 2a shows the high-voltage transmission grid of Great Britain as of January 2023, totalling 630 nodes (representing power stations, substations, and line intersections) and 763 edges with their operating voltages. Of the roughly 1300 power stations dotted around the island, we include those 38 with installed capacities of at least 400 MW that are directly connected to the national grid [32]; following [5, 35] we give all other nodes a random value $P_i \sim \mathcal{U}[-200, +200]$ such that $\sum_i P_i = 0$.

(a) Densities on edges with highest relative error



(b) True (black) and predicted network response

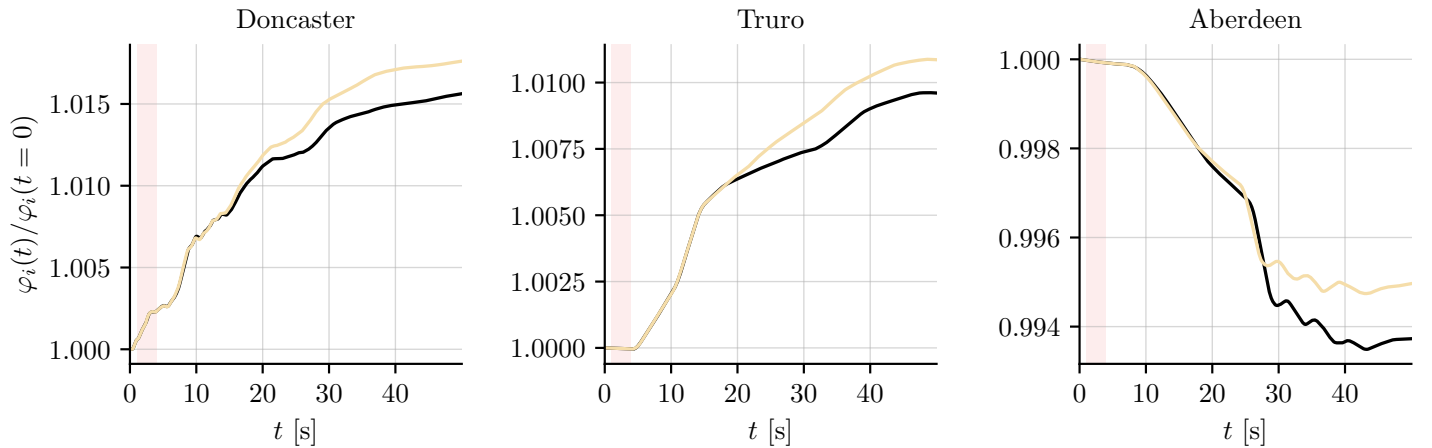


Figure 3: Estimating the line failure location. (a) The densities on four edges with the highest relative prediction error $|\hat{a}_{ij} - a_{ij}^0|/a_{ij}^0$ and their respective p -values for measuring the unperturbed value a_{ij}^0 . Red dotted lines indicate the values of the unperturbed network, green lines the expectation values of the distributions. The marginals are smoothed using a Gaussian kernel. We use a training set of length $L = 400$ steps, and the batch size is $B = 2$. CPU runtime: 24 minutes. (b) True (black) and predicted network responses at three different locations in the network. The responses are each normalised to the value at $t = 0$. The shaded area represents the 400 time steps used to train the model. While the model is able to perfectly fit the response within the training range, it is not able to learn the full network from insufficient data, causing the time series to diverge for larger t .

We simulate a power cut in the northeast of England by iterating the Kuramoto dynamics until the system reaches a steady state of equilibrium (defined as $|\dot{\varphi}_i|/\varphi_i \leq 0.01 \forall i$) and then removing two links and recording the network response (fig. 2b). From the response we can infer the adjacency matrix of the perturbed network $\tilde{\mathbf{A}}$ (with missing links) and, by comparing with \mathbf{A}^0 , the line failure locations.

We let a neural network output a (vectorised) adja-

gency matrix $\hat{\mathbf{A}}$ and use this estimated adjacency matrix to run the differential equation eq. [4], which will produce an estimate of the phase vector $\hat{\varphi}$. A hyperparameter sweep on synthetic data showed that using a deep neural network with 5 layers, 20 nodes per layer, and no bias provides optimal results. We use the hyperbolic tangent as an activation function on each layer except

the last, where we use the ‘hard sigmoid’

$$\sigma(x) = \begin{cases} 0, & x \leq -3, \\ 1, & x \geq +3, \\ x/6 + 1/2, & \text{else,} \end{cases}$$

which allows neural net output components to actually become zero, and not just asymptotically close, thereby ensuring sparsity of the adjacency matrix. We use the Adam optimizer [26] with a learning rate of 0.002 for the gradient descent step, and initialise the neural network’s weights with a prior $\pi^0(\boldsymbol{\theta})$ in such a way that the prior $\pi^0(\hat{\mathbf{A}})$ is a delta distribution on the complete graph, $\pi(\hat{a}_{ij}) \sim \delta(1) \forall i, j$. This maximises the sampling domain on each edge. Since the neural network outputs are in $[0, 1]$, we scale the network weights $a_{ij} \rightarrow \lambda a_{ij}$ such that $a_{ij} \in [0, 1]$, and absorb λ into the coupling constant κ ; see the Supplementary Information for details on the calculations.

We use the following loss function $J(\hat{\mathbf{A}})$ to train the internal weights $\boldsymbol{\theta}$ of the neural network such that it will output an adjacency matrix that reproduces the observed data:

$$J(\hat{\mathbf{A}}) = \|\hat{\boldsymbol{\varphi}}(\hat{\mathbf{A}}) - \boldsymbol{\varphi}\|_2 + \|\hat{\mathbf{A}} - \hat{\mathbf{A}}^T\|_2 + \text{tr}(\hat{\mathbf{A}}) + \nu \|\hat{\mathbf{A}} - \mathbf{A}^0\|_2.$$

The first term is the error on the data, the second penalises asymmetry to enforce undirectedness of the network, and the third sets the diagonal to zero (which cannot be inferred from the data). ν is a function designed to let the neural network search for $\tilde{\mathbf{A}}$ in the vicinity of \mathbf{A}^0 , since we can assume a priori that the two will be similar in most entries. To this end we set $\nu = 10$ while $|\langle \partial_s J \rangle| > 10^{-10}$ and $|\langle \partial_{ss} J \rangle| > 10^{-10}$, and $\nu = 0$ thereafter, where s is the iteration count (number of training steps), and $\langle J \rangle$ the total loss averaged over a window of 20 iterations, see fig. 4. In other words, we push the neural network towards a stable minimum in the neighbourhood of \mathbf{A}^0 and, once the loss stabilises, permanently set $\nu = 0$.

In theory $L = N - 1$ observations are needed to completely infer the network, though symmetries in the data usually means $L > N$ is required in practice [38]. Traditional regression methods are not applicable in the underdetermined case $L < N - 1$, since they involve inversion of the Gram matrix $\mathbf{G}_i \mathbf{G}_i^T$, $\mathbf{G}_i \in \mathbb{R}^{N \times L}$ containing

all L interactions of the i -th node with all other nodes, and additional constraints (e.g. sparsity assumptions) must thus be placed on the network to infer its topology [39]. We purposefully underdetermine the problem by only using $L < N - 1$ steps, leading to an average Gram matrix rank of 6 (about 100 times less than required for complete inference). Additionally, we train the network on data recorded 1 second after the power cut, where many nodes will still be close to equilibrium. Our method does not involve matrix inversion, and can thus deal naturally with non-convex problems. Though the neural network may be unable to completely infer the network, it can nevertheless produce a density $\rho(\hat{\mathbf{A}})$, recorded during the training, that allows us to perform hypothesis testing on the line failure location.

We show the results in fig. 3, where we plot the densities on the four network edges with the highest relative prediction error $|\hat{a}_{ij} - a_{ij}^0|/a_{ij}^0$, \hat{a}_{ij} being the most likely value. The advantage of obtaining uncertainty quantification on the network is now immediately clear: even in the underdetermined case we are able to make meaningful statistical statements about the line failure location. We see that the missing edges consistently have the highest relative prediction errors, and that the p -values for measuring the unperturbed value a_{ij}^0 are around 5%, while being statistically insignificant for all other edges. It is interesting to note that the other candidate locations are also within the vicinity of the line failure, though their predicted values are much closer to the unperturbed value. In fig. 3b, we see that

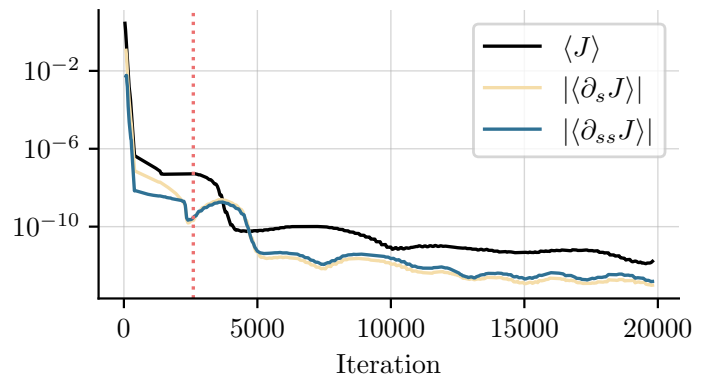


Figure 4: The total loss J and its derivatives $\partial_s J$ and $\partial_{ss} J$, averaged over a window of 20 iterations. The red dotted line indicates the value at which ν is set to 0.

the predicted network reproduces the response dynamics for the range covered by the training data when inserted into eq. [4], but, since the problem was purposefully underdetermined, the errors in the prediction $\hat{\mathbf{A}}$ cause the predicted and true time series to diverge for larger t . Densities were obtained in about twenty minutes on a regular laptop CPU.

III. Inferring economic cost networks from noisy data

In the previous example the underlying network was a physical entity, but in many cases networks model abstract connections. We therefore now consider a commonly used economic model of the coupling of supply and demand [12, 13, 43] and a dataset of economic activity across Greater London. The goal is to learn the entire coupling network, not just to infer the (non-)existence of individual edges. In the model, N origin zones, representing economic demand, are coupled to M destination zones, modelling the supply side, through a network whose weights quantify the convenience with which demand from zone i can be supplied from zone j : the higher the weight, the more demand flows through that edge (see fig. 5a). Such a model is applicable e.g. to an urban setting [12], the origin zones representing residential areas, the destination zones e.g. commercial centres, and the weights quantifying the connectivity between the two (transport times, distances, etc.). The resulting cumulative demand at destination zone j depends both on the current size $W_j(t)$ of the destination zone and the network weights c_{ij} :

$$D_j = \sum_{i=1}^N \frac{W_j(t)^\alpha c_{ij}^\beta}{\sum_{k=1}^M W_k(t)^\alpha c_{ik}^\beta} O_i(t).$$

The sizes W_j are governed by a system of M coupled logistic

Stratonovich stochastic differential equations

$$dW_j = \epsilon W_j (D_j - \kappa W_j) dt + \sigma W_j \circ dB_j,$$

with given initial conditions $W_j(0)$, see fig. 5a. α , β , κ , and ϵ are scalar parameters. Our goal is to infer the connectivities c_{ij} from observations of the time series $\mathbf{O}(t)$ and $\mathbf{W}(t)$. The model includes multiplicative noise B_j with variance $\sigma \geq 0$, with \circ signifying Stratonovich

integration. Crucially, the model depends non-linearly on the network \mathbf{C} : classical regression methods are thus not applicable here.

We apply this model to a previously studied dataset of economic activity in Greater London [13, 25]. We use the ward-level household income from $N = 625$ wards for 2015 [41] and the retail floor space of the $M = 49$ largest commercial centres in London [40] as the initial origin zone and destination zone sizes respectively, i.e. $\mathbf{O}(0)$ and $\mathbf{W}(0)$, and from this generate a synthetic time series using the parameters estimated in [25] for a high noise level of $\sigma = 0.14$. For the network \mathbf{C} we use the Google Distance Matrix API¹ to extract the shortest travel time d_{ij} between nodes, using either public transport or driving. The network weights are derived in [44] as

$$c_{ij} = e^{-d_{ij}/\tau}$$

where the scale factor $\tau = \sup_{i,j} d_{ij}$ ensures a unitless exponent.

We generate a synthetic time series of length $L = 10000$ from which we subsample 2500 2-step windows, giving a total training set size of 5000. This is to ensure we sample a sufficiently broad spectrum of the system's dynamics, thereby fully determining the inference problem and isolating the effect of the training noise. A hyperparameter sweep on synthetic data showed that using a neural network with 2 layers, 20 nodes per layer, and no bias yields optimal results. We use the hyperbolic tangent as the activation function on all layers except the last, where we use the standard sigmoid function (since the network is complete, there is no need to use the hard sigmoid, since all edges are nonzero). To train the neural network we use the simple loss function

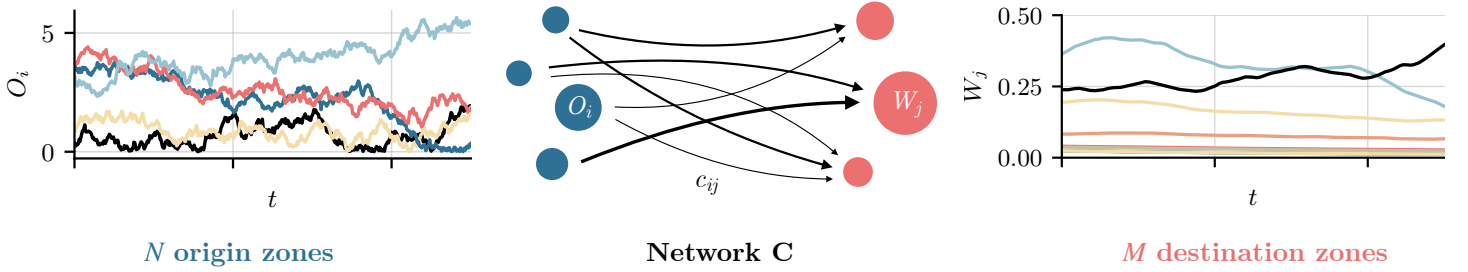
$$J_\theta(\hat{\mathbf{A}}) = \|\hat{\varphi}(\hat{\mathbf{A}}) - \varphi\|_2.$$

Since the dynamics are invariant under scaling of $\mathbf{C} \rightarrow \lambda \mathbf{C}$, we normalise the rowsums of the predicted and true networks, $\sum_j c_{ij} = 1$.

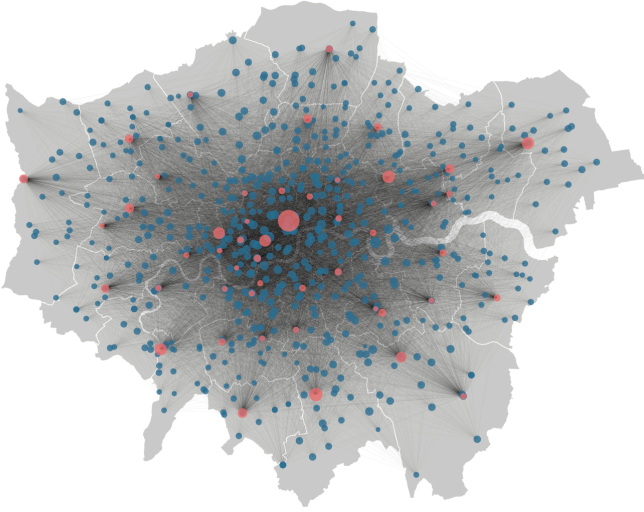
Figure 5c shows the inferred distribution $P(k)$ of the (weighted) origin zone node degrees $k_i = \sum_j c_{ij}$. The solid line is the maximum likelihood prediction, and the dotted red line the true distribution. Even with a high level of noise, the model manages to accurately predict the underlying connectivity matrix, comprising over

¹developers.google.com/maps/documentation/distance-matrix

(a) Model dynamics



(b) Initial data and travel times network



(c) Inferred weighted degree distribution

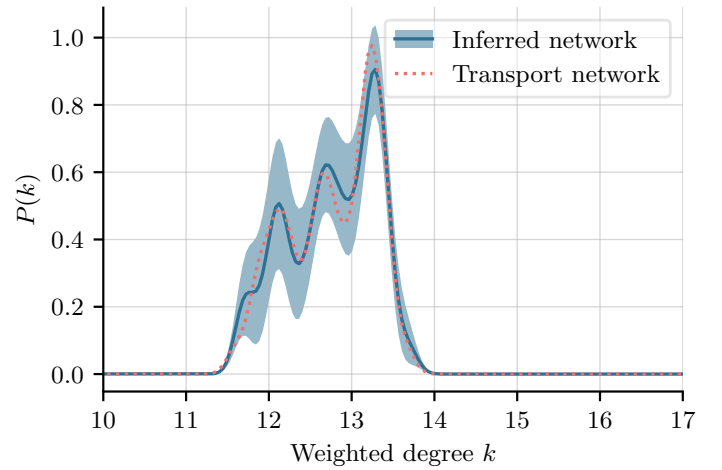


Figure 5: Inferring economic cost networks. (a) In the model, N origin zones (red) are connected to M destination zones (blue) through a weighted directed network. Economic demand flows from the origin zones to the destination zones, which supply the demand. We model the origin zones $O_i(t)$ as a Wiener process with variance $\sigma_O = 0.1$. The resulting cumulative demand at destination zone j is given by W_j . Note that the origin zone sizes fluctuate more rapidly than the destination zones, since there is a delay in the destination zones' response to changing consumer patterns, controlled by the parameter ϵ . We use the parameters as estimated in [25], $\alpha = 0.92$, $\beta = 0.54$, $\kappa = 8.3$, and set $\epsilon = 2$. (b) The initial origin and destination zone sizes, given by the total household income of the $N = 629$ wards in London (blue nodes) and the retail floor space of $M = 49$ major centres (red nodes) [40, 41]. The network is given by travel times as detailed in the text. Background map: [42]. (c) Predicted degree distribution (solid line) of the inferred network, for a high noise level of $\sigma = 0.14$, with Hellinger uncertainty eq. [5] (shaded area), and the true distribution (red dotted line). CPU runtime: 3 min 41 s.

30,000 weights, in under 5 minutes on a regular laptop CPU. We quantify the uncertainty on the distribution using the Hellinger metric,

$$\bar{d}_H(k) \sim \int \left(\sqrt{\hat{\rho}(k)} - \sqrt{\hat{\rho}(k | \hat{\mathbf{T}})} \right)^2 \exp(-\|\hat{\mathbf{T}} - \mathbf{T}\|_2) d\hat{\mathbf{T}}. \quad (5)$$

Here, we define the maximum likelihood estimate as the predicted density $\hat{\rho}(k)$ for which uncertainty is to be calculated. As we will discuss in the last section, this method meaningfully captures the uncertainty due to the noise in the data.

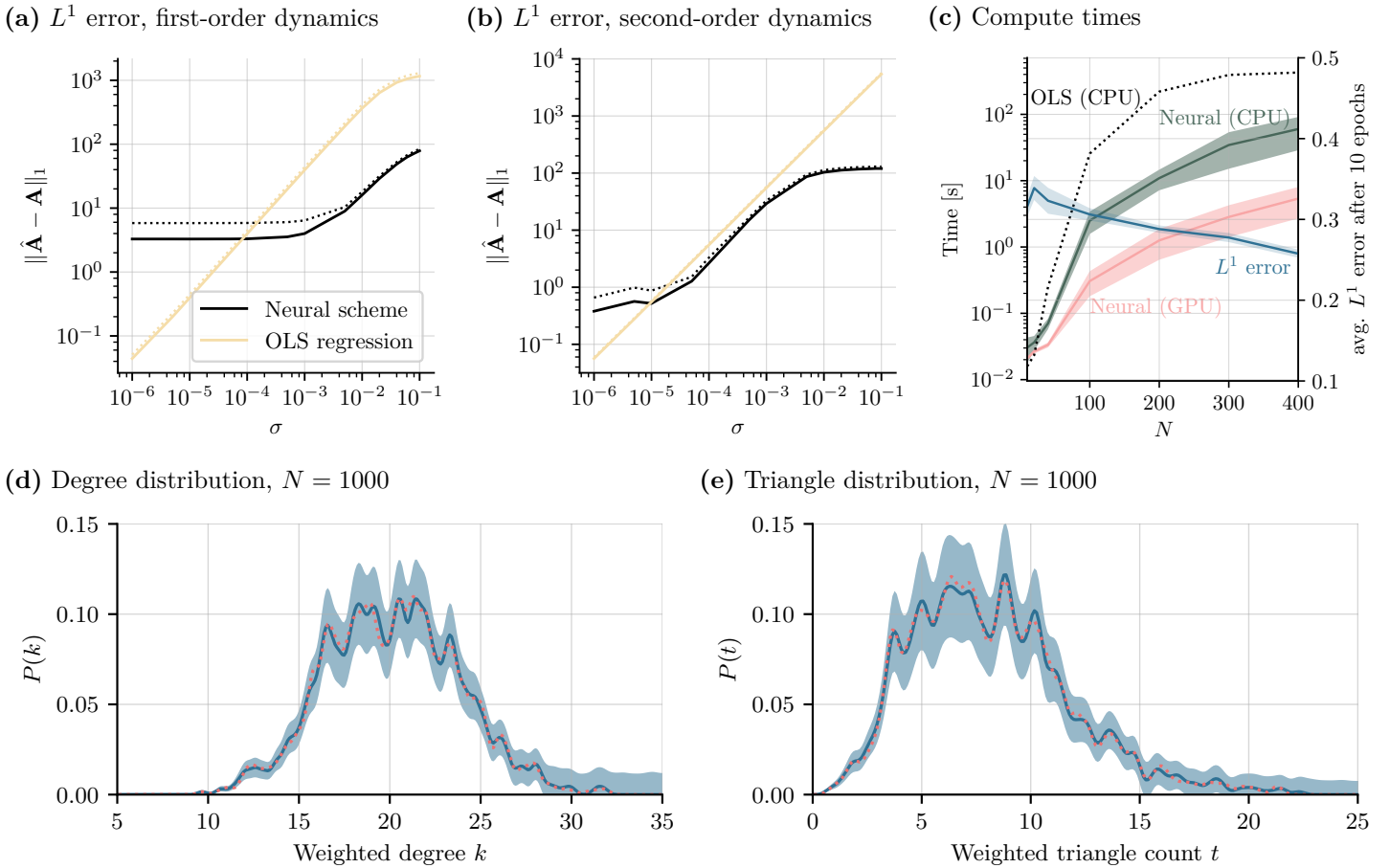


Figure 6: Computational performance analysis. **(a)** L^1 prediction error of the neural scheme (black) and OLS as a function of the noise variance σ on the training data. For very high noise levels, the training data is essentially pure noise, and the prediction errors begin to plateau. First-order Kuramoto dynamics are used ($\alpha = 0$). **(b)** The same plot as in (a), but using second-order dynamics (with $\alpha = 1$). **(c)** Compute times for a single epoch of the neural method as a function of the network size N . Shown are the compute times on a standard CPU (Apple M1, green line) and GPU (Nvidia GeForce RTX 3090, pink line), averaged over 100 runs, with the shaded areas showing one standard deviation. Also shown is the compute time for complete inference using ordinary least squares (black dotted line), which scales as N^3 (note the logarithmic axis). On the right axis, the average L^1 prediction error $\frac{1}{N}\|\hat{\mathbf{A}} - \mathbf{A}\|_1$ of the neural scheme after 10 epochs is shown, which remains fairly constant as a function of N , showing that the number of gradient descent steps required to achieve a given average prediction error does not depend on N . **(d)** Predicted degree distribution and **(e)** triangle distribution of an inferred network, trained on first-order noisy Kuramoto data ($\sigma = 0.001$). The blue shaded areas indicate the Hellinger uncertainty eq. [5], and the red dotted lines are the true distributions. CPU runtime: 1 hour 3 minutes.

IV. Performance analysis and comparison with OLS

We now analyse our method’s performance, both in terms of prediction quality and computational speed, by comparing it to that of a classical regression method, presented e.g. in [6, 39]. As mentioned in the introduction, more efficient network learning methodologies have been

developed for specific problems; however, we compare our method with OLS since both methods are general and do not rely on a specific data structure.

Consider noisy Kuramoto dynamics,

$$\alpha \frac{d^2 \varphi_i}{dt^2} + \frac{d\varphi_i}{dt} = \omega_i + \sum_j a_{ij} \sin(\varphi_j - \varphi_i) + \xi_i, \quad (6)$$

with $\xi_i \stackrel{iid}{\sim} \mathcal{N}(0, \sigma)$, and ω_i the eigenfrequencies of the

nodes. Gathering the L terms on the left side into a single vector \mathbf{X}_i for each node, we obtain N equations

$$\mathbf{X}_i = \mathbf{A}_i \cdot \mathbf{G}_i + \epsilon_i, \quad (7)$$

with $\mathbf{X}_i \in \mathbb{R}^{1 \times L}$, $\mathbf{A}_i \in \mathbb{R}^{1 \times N}$ the i -th row of \mathbf{A} , and $\mathbf{G}_i \in \mathbb{R}^{N \times L}$ the L observations of the i -th column of \mathbf{G} . From this we can then naturally estimate the i -th row of \mathbf{A} using ordinary least squares:

$$\hat{\mathbf{A}}_i = \operatorname{argmin}_{\gamma \in \mathbb{R}^{1 \times N}} \|\mathbf{X}_i - \gamma \cdot \mathbf{G}_i\|_2^2 = \mathbf{X}_i \mathbf{G}_i^T (\mathbf{G}_i \mathbf{G}_i^T)^{-1}. \quad (8)$$

Given sufficiently many linearly independent observations, the Gram matrix $\mathbf{G}_i \mathbf{G}_i^T$ will be invertible and the network can be inferred (with the diagonal manually set to 0). We use synthetic Kuramoto data to compare our method’s performance to that of OLS. In order to ensure invertibility of $\mathbf{G}_i \mathbf{G}_i^T$, we generate $L \gtrsim N/2$ datasets of 2 time steps each.

Figures 6a–b show our method’s prediction accuracy alongside that of OLS regression as a function of the noise σ on the training data; the accuracy here is defined as the L^1 error

$$\|\hat{\mathbf{A}} - \mathbf{A}\|_1 = \sum_{i,j} |\hat{a}_{ij} - a_{ij}|.$$

For the practically noiseless case of $\sigma < 10^{-5}$, the regression scheme on average outperforms the neural approach; however, even for very low noise levels $\sigma \geq 10^{-5}$ and above, the neural approach proves far more robust, outperforming OLS by up to one order of magnitude and maintaining its prediction performance up to low noise levels of $\sigma \leq 10^{-3}$. These results hold both for first-order ($\alpha = 0$) and second-order Kuramoto equations [4] (see fig. 6b); in the second-order case, the neural method begins outperforming OLS at even lower levels of σ than in the first-order case, though the improvement is not as significant.

In figure 6c we show the average training time per epoch as a function of N , with training conducted both on a standard laptop CPU and a standard GPU. Each epoch of the model equation requires $\mathcal{O}(LN^2)$ operations for the vector-matrix multiplication in eq. [8], and $\mathcal{O}(LN^2/B)$ for the stochastic gradient descent update, where we are holding L/B constant to ensure comparability. We thus obtain an algorithmic complexity of $\mathcal{O}(LN^2)$. As is visible, the average L^1 error per edge

weight remains constant over N , indicating that the number of gradient descent steps required to achieve a given node-averaged prediction accuracy is independent of N . The total complexity of our method is thus $\mathcal{O}(n_E \times LN^2)$, with n_E the number of training epochs. By comparison, OLS in general has a cubic dependency on N , due to the required matrix inversion. Being a neural approach, our method can make use of GPU accelerated training, leading to an order of magnitude faster performance.

Lastly, figures 6d–e show the estimated weighted degree and triangle distributions of a graph with 1000 nodes, or 1 million edge weights to be estimated, for noisy training data. The number of weighted, undirected triangles on each node i is given by $\frac{1}{2} \sum_{jk} a_{ij} a_{jk} a_{ki}$. The model robustly finds the true adjacency matrix, and we again quantify uncertainty on the prediction using the Hellinger distance (eq. [5]) between each distribution estimated during training and the maximum likelihood estimate. Estimating a network with 1000 nodes on a standard laptop CPU took about 1 hour, which reduces to 6 minutes when using a GPU. Most high-performance network inference techniques demonstrate their viability on graphs with at most this number of nodes, e.g. ConNIE [17] and NetINF [19]. In [17], the authors state that graphs with 1000 nodes can typically be inferred from cascade data in under 10 minutes on a standard laptop. Similarly, the authors of NetINF [19] state that it can infer a network with 1000 nodes in a matter of minutes, though this algorithm does not infer edge weights, only the existence of edges, and neither technique provides uncertainty quantification.

V. Quantifying uncertainty

There are two sources of uncertainty when inferring adjacency matrices: the non-convexity of the loss function J , and the noise σ on the data. In general, it is hard to quantify the convexity of J , since we do not know how many networks fit the equation at hand. However, when the dynamics are linear in the adjacency matrix \mathbf{A} , we can do so using the Gram matrix of the observations of each node i , $\mathbf{G}_i \mathbf{G}_i^T$. For regression methods to be applicable, $\mathbf{G}_i \mathbf{G}_i^T$ must be invertible for each i . The (non-)convexity of the problem can thus be quantified for example by the minimum rank of all the Gram

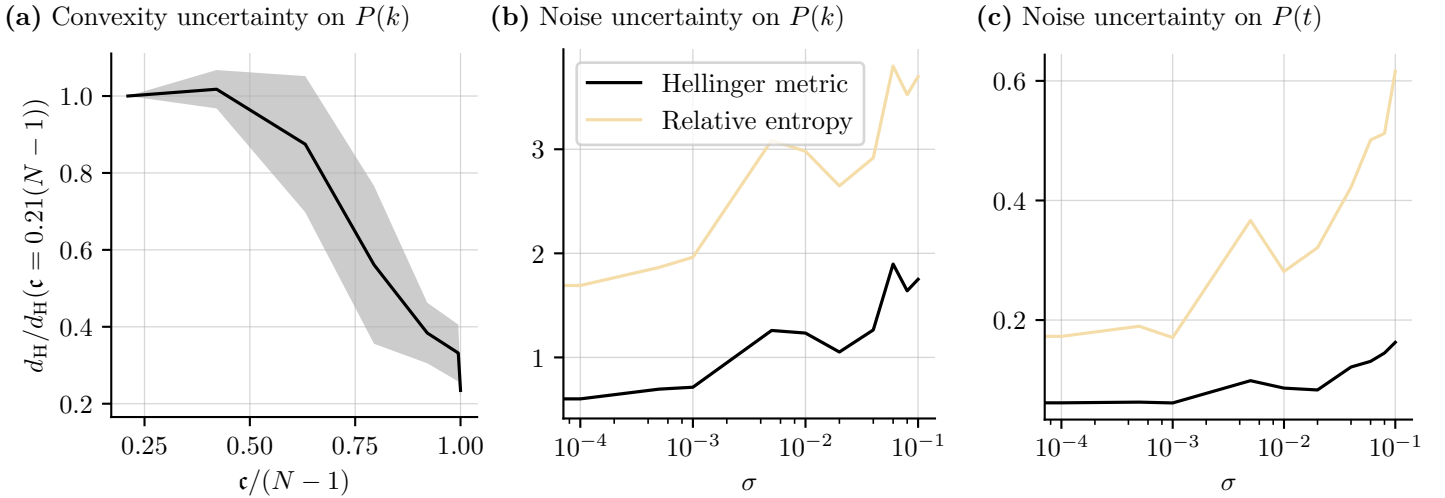


Figure 7: Quantifying the two types of uncertainty: **(a)** Total Hellinger error on the degree distribution $P(k)$ as a function of \mathbf{c} (eq. [9]) in the noiseless case. The error is normalised to the value at $\mathbf{c} = 0.21(N-1)$. As \mathbf{c} increases, the error on the prediction decreases almost linearly. We run the model from 10 different initialisations and average over each (shaded area: standard deviation). **(b)** and **(c)**: Prediction uncertainty due to noise in the data. Shown are the average Hellinger error (eq. [5]) and average relative entropy (eq. [10]) to the maximum likelihood estimate for the degree distribution $P(k)$ and triangle distribution $P(t)$ as a function of the noise σ in the data. Each line is an average over 10 different initialisations. In all cases, training was conducted on synthetic, first-order Kuramoto data (eq. [6] with $\alpha = 0$).

matrices,

$$\mathbf{c} := \min_i \text{rk}(\mathbf{G}_i \mathbf{G}_i^T). \quad (9)$$

The problem is fully determined if $\mathbf{c} = N-1$. In figure 7a we show the Hellinger uncertainty eq. [5] on the predicted degree distribution as a function of \mathbf{c} . As is visible, the error on the distribution decreases almost linearly as \mathbf{c} tends to its maximum value $N-1$. For $\mathbf{c} = N-1$, some residual uncertainty remains due to the uncertainty on the neural network parameters θ .

In figures 7b–c we again show the Hellinger error on the predicted degree and triangle distributions, this time as a function of the noise σ . To demonstrate that the uncertainty is not an artefact of the choice of metric, we also show the behaviour of the relative entropy,

$$\begin{aligned} \bar{d}_{\text{KL}}(k) \sim \\ \int \hat{\rho}(k | \hat{\mathbf{T}}) \log \left(\frac{\hat{\rho}(k | \hat{\mathbf{T}})}{\hat{\rho}(k)} \right) \exp(-\|\hat{\mathbf{T}} - \mathbf{T}\|_2) d\hat{\mathbf{T}}. \end{aligned} \quad (10)$$

Both metrics reflect the noise on the training data, providing similarly behaved, meaningful uncertainty quantification. As the noise tends to 0, some residual uncertainty again remains. Our method thus manages to

capture the uncertainty arising from both sources: the non-convexity of J and the noise σ on the data.

VI. Discussion

In this work we have demonstrated a performative method to estimate network adjacency matrices from time series data. We showed its effectiveness at correctly and reliably inferring networks in a variety of scenarios: convex and non-convex cases, low to high noise regimes, and equations that are both linear and non-linear in \mathbf{A} . We were able to reliably infer power line failures in the national power grid of Great Britain, and the connectivity matrix of an economic system covering all of Greater London. We showed that our method is well able to handle inference of hundreds of thousands to a million edge weights, while simultaneously giving uncertainty quantification that meaningfully reflects both the non-convexity of the loss function as well as the noise on the training data. Our method outperforms classical ordinary least squares regression, both in terms of prediction accuracy and computational speed, while extending to the case of non-linear dynamics. In conjunction with our previous work [25], we have now also demonstrated the

viability of using neural networks for parameter calibration in both the low- and high-dimensional case. Our method is simple to implement as well as highly versatile, giving excellent results across a variety of problems. All experiments in this work were purposefully conducted on a standard laptop CPU, typically taking on the order of minutes to run; however, being a neural scheme, our method can make use of GPU acceleration, further reducing the compute times.

Many lines for future research open up from this work. Firstly, a thorough theoretical investigation of the method and a more quantitative comparison to other, similar methods is warranted, e.g. approximate Bayesian computing [45, 46], physics-informed neural networks [47], and using dropout for uncertainty quantification in neural networks [48]. Another direction is further reducing the amount of data required to learn parameters, which in many applications may not be abundantly available, and in future research the authors aim to address the question of learning systems properties from observations of a single particle trajectory at the mean-field limit [49, 50].

Data, materials, and Software Availability Code and synthetic data can be found under <https://github.com/ThGaskin/NeuralABM>. It is easily adaptable to new models and ideas. The code uses the `utopya` package² [51, 52] to handle simulation configuration and efficiently read, write, analyse, and evaluate data. This means that the model can be run by modifying simple and intuitive configuration files, without touching code. Multiple training runs and parameter sweeps are automatically parallelised. The neural core is implemented using `pytorch`³. All synthetic datasets as well as the London dataset have been made available, together with the configuration files needed to reproduce the plots. Detailed instructions are provided in the supplementary material and the repository. The British power grid data [29–31] is property of the respective organisations and cannot be made available without permission; however, as of early 2023 it is freely available from those organisations upon request. The code used to run the experiments is

available in the repository.

Acknowledgements The authors are grateful to Dr Andrew Duncan for the fruitful discussions on power grid dynamics. TG was funded by the University of Cambridge School of Physical Sciences VC Award via DAMTP and the Department of Engineering, and supported by EPSRC grants EP/P020720/2 and EP/R018413/2. The work of GP was partially funded by EPSRC grant EP/P031587/1, and by J.P. Morgan Chase & Co through a Faculty Research Award 2019 and 2021. MG was supported by EPSRC grants EP/T000414/1, EP/R018413/2, EP/P020720/2, EP/R034710/1, EP/R004889/1, and a Royal Academy of Engineering Research Chair.

References

- [1] SW Simard, et al., Mycorrhizal networks: Mechanisms, ecology and modelling. *Fungal Biology Reviews* **26**, 39–60 (2012).
- [2] C Hettenhausen, et al., Stem parasitic plant *cuscuta australis* (dodder) transfers herbivory-induced signals among plants. *Proceedings of the National Academy of Sciences* **114**, E6703–E6709 (2017).
- [3] D Brockmann, D Helbing, The hidden geometry of complex, network-driven contagion phenomena. *Science* **342**, 1337–1342 (2013).
- [4] N Molkenthin, M Schröder, M Timme, Scaling laws of collective ride-sharing dynamics. *Physical Review Letters* **125** (2020).
- [5] I Simonsen, L Buzna, K Peters, S Bornholdt, D Helbing, Transient dynamics increasing network vulnerability to cascading failures. *Physical Review Letters* **100** (2008).
- [6] SG Shandilya, M Timme, Inferring network topology from complex dynamics. *New Journal of Physics* **13**, 013004 (2011).
- [7] U Stelzl, et al., A human protein-protein interaction network: A resource for annotating the proteome. *Cell* **122**, 957–968 (2005).
- [8] SR Proulx, DE Promislow, PC Phillips, Network thinking in ecology and evolution. *Trends in Ecology & Evolution* **20**, 345–353 (2005) Special issue: Bumper book review.
- [9] S Allesina, D Alonso, M Pascual, A general model for food web structure. *Science* **320**, 658–661 (2008).

²utopia-project.org, utopya.readthedocs.io/en/latest

³pytorch.org

- [10] J Tegnér, MKS Yeung, J Hasty, JJ Collins, Reverse engineering gene networks: Integrating genetic perturbations with dynamical modeling. *Proceedings of the National Academy of Sciences* **100**, 5944–5949 (2003).
- [11] BO Palsson, *Systems Biology: Properties of Reconstructed Networks*. (Cambridge University Press, New York, NY, USA), (2006).
- [12] M Batty, R Milton, A new framework for very large-scale urban modelling. *Urban Studies* **58**, 3071–3094 (2021).
- [13] L Ellam, M Girolami, GA Pavliotis, A Wilson, Stochastic modelling of urban structure. *Proceedings of the Royal Society A: Mathematical, Physical and Engineering Sciences* **474**, 20170700 (2018).
- [14] MD Vicario, et al., The spreading of misinformation online. *Proceedings of the National Academy of Sciences* **113**, 554–559 (2016).
- [15] S Aral, L Muchnik, A Sundararajan, Engineering social contagions: Optimal network seeding in the presence of homophily. *Network Science* **1**, 125–153 (2013).
- [16] S Vosoughi, D Roy, S Aral, The spread of true and false news online. *Science* **359**, 1146–1151 (2018).
- [17] SA Myers, J Leskovec, On the convexity of latent social network inference in *Proceedings of the 23rd International Conference on Neural Information Processing Systems - Volume 2*, NIPS’10. (Curran Associates Inc., Red Hook, NY, USA), pp. 1741–1749 (2010).
- [18] M Gomez-Rodriguez, D Balduzzi, B Schölkopf, Uncovering the temporal dynamics of diffusion networks in *Proceedings of the 28th International Conference on International Conference on Machine Learning*, ICML’11. (Omnipress, Madison, WI, USA), pp. 561–568 (2011).
- [19] M Gomez-Rodriguez, J Leskovec, A Krause, Inferring networks of diffusion and influence. *ACM Transactions on Knowledge Discovery from Data* **5**, 1–37 (2012).
- [20] VA Makarov, F Panetsos, O de Feo, A method for determining neural connectivity and inferring the underlying network dynamics using extracellular spike recordings. *Journal of Neuroscience Methods* **144**, 265–279 (2005).
- [21] FV Bussel, Inferring synaptic connectivity from spatio-temporal spike patterns. *Frontiers in Computational Neuroscience* **5** (2011).
- [22] N Meinshausen, P Bühlmann, High-dimensional graphs and variable selection with the Lasso. *The Annals of Statistics* **34**, 1436 – 1462 (2006).
- [23] M Yuan, Y Lin, Model selection and estimation in the Gaussian graphical model. *Biometrika* **94**, 19–35 (2007).
- [24] M Timme, J Casadiego, Revealing networks from dynamics: an introduction. *Journal of Physics A: Mathematical and Theoretical* **47**, 343001 (2014).
- [25] T Gaskin, GA Pavliotis, M Girolami, Neural parameter calibration for large-scale multi-agent models. *Proceedings of the National Academy of Sciences* **120** (2023).
- [26] DP Kingma, J Ba, Adam: A Method for Stochastic Optimization. *arXiv* **1412.6980** [cs.LG] (2014).
- [27] S Geman, D Geman, Stochastic Relaxation, Gibbs Distributions, and the Bayesian Restoration of Images. *IEEE Transactions on Pattern Analysis and Machine Intelligence* **PAMI-6**, 721–741 (1984).
- [28] AM Stuart, Inverse problems: A Bayesian perspective. *Acta Numerica* **19**, 451–559 (2010).
- [29] National Grid, Transmission Network Shapefiles (<https://www.nationalgrid.com/electricity-transmission/network-and-infrastructure/network-route-maps>) (2023).
- [30] SP Energy Networks, Transmission Network GIS Shapefiles (https://www.spenergynetworks.co.uk/pages/utility_map_viewer.aspx) (2023).
- [31] Scottish and Southern Electricity Networks, Transmission Network GIS Shapefiles (<https://www.ssen.co.uk/globalassets/library/connections---useful-documents/network-maps/5-gis-guide-shape-files-v1.pdf>) (2023).
- [32] Department for Business, Energy and Industrial Strategy, Digest of UK Energy Statistics 5: Electricity (2022).
- [33] Y Kuramoto, Self-entrainment of a population of coupled non-linear oscillators in *International Symposium on Mathematical Problems in Theoretical Physics*, ed. H Araki. (Springer-Verlag), pp. 420–422 (1975).
- [34] G Filatrella, AH Nielsen, NF Pedersen, Analysis of a power grid using a Kuramoto-like model. *The European Physical Journal B* **61**, 485–491 (2008).
- [35] M Rohden, A Sorge, M Timme, D Witthaut, Self-organized synchronization in decentralized power grids. *Phys. Rev. Lett.* **109**, 064101 (2012).
- [36] T Nishikawa, AE Motter, Comparative analysis of existing models for power-grid synchronization. *New Journal of Physics* **17**, 015012 (2015).
- [37] YP Choi, Z Li, Synchronization of nonuniform Kuramoto oscillators for power grids with general connectivity and dampings. *Nonlinearity* **32**, 559–583 (2019).

- [38] F Basiri, J Casadiego, M Timme, D Witthaut, Inferring power-grid topology in the face of uncertainties. *Phys. Rev. E* **98**, 012305 (2018).
- [39] M Timme, Revealing network connectivity from response dynamics. *Physical Review Letters* **98**, 224101 (2007).
- [40] Greater London Authority, 2017 Health Check Report (2017).
- [41] Greater London Authority, 2015 ward profiles and atlas (2015) Online.
- [42] Greater London Authority, Statistical boundary files for London (2011).
- [43] B Harris, AG Wilson, Equilibrium values and dynamics of attractiveness terms in production-constrained spatial-interaction models. *Environment and Planning A: Economy and Space* **10**, 371–388 (1978).
- [44] A Wilson, A statistical theory of spatial distribution models. *Transportation Research* **1**, 253–269 (1967).
- [45] K Csilléry, MG Blum, OE Gaggiotti, O François, Approximate Bayesian Computation (ABC) in practice. *Trends in Ecology & Evolution* **25**, 410–418 (2010).
- [46] E Jennings, M Madigan, astroABC: An Approximate Bayesian Computation Sequential Monte Carlo sampler for cosmological parameter estimation. *Astronomy and Computing* **19**, 16–22 (2017).
- [47] M Raissi, P Perdikaris, G Karniadakis, Physics-informed neural networks: A deep learning framework for solving forward and inverse problems involving nonlinear partial differential equations. *Journal of Computational Physics* **378**, 686–707 (2019).
- [48] Y Gal, Z Ghahramani, Dropout as a Bayesian Approximation: Representing Model Uncertainty in Deep Learning. *Proceedings of The 33rd International Conference on Machine Learning* **48**, 1050–1059 (2016).
- [49] GA Pavliotis, A Zandoni, A method of moments estimator for interacting particle systems and their mean field limit. *arXiv* **2212.00403 [math.NA]** (2022).
- [50] N Zagli, GA Pavliotis, V Lucarini, A Alecio, Dimension reduction of noisy interacting systems. *Phys. Rev. Res.* **5**, 013078 (2023).
- [51] L Riedel, B Herdeanu, H Mack, Y Sevinchan, J Weninger, Utopia: A comprehensive and collaborative modeling framework for complex and evolving systems. *Journal of Open Source Software* **5**, 2165 (2020).
- [52] Y Sevinchan, B Herdeanu, J Traub, dantro: a python package for handling, transforming, and visualizing hierarchically structured data. *Journal of Open Source Software* **5**, 2316 (2020).
- [53] National Grid ESO, What is Frequency? (<https://www.nationalgrideso.com/electricity-explained/how-do-we-balance-grid/what-frequency>) (2023).

Supporting Information

Neural networks: Notation and Terminology

A *neural network* is a sequence of length $L \geq 1$ of concatenated transformations. Each *layer* of the net consists of L_i *neurons*, connected through a sequence of *weight matrices* $\mathbf{W}_i \in \mathbb{R}^{L_{i+1} \times L_i}$. Each layer applies the transformation

$$\sigma_i(\mathbf{W}_i \mathbf{x} + \mathbf{b}_i)$$

to the input \mathbf{x} from the previous layer, where $\mathbf{b}_i \in \mathbb{R}^{L_{i+1}}$ is the *bias* of the i -th layer. The function $\sigma_i : \mathbb{R}^{L_{i+1}} \rightarrow \mathbb{R}^{L_{i+1}}$ is the *activation function*; popular choices include the *rectified linear unit* (ReLU) activation function $\sigma(x) = \max(x, 0)$, and the *sigmoid activation function* $\sigma(x) = (1 + e^{-x})^{-1}$. A neural net has an *input layer*, an *output layer*, and *hidden layers*, which are the layers in between the in- and output layers. If a network only has one hidden layer, we call it *shallow*, else we call the neural net *deep*.

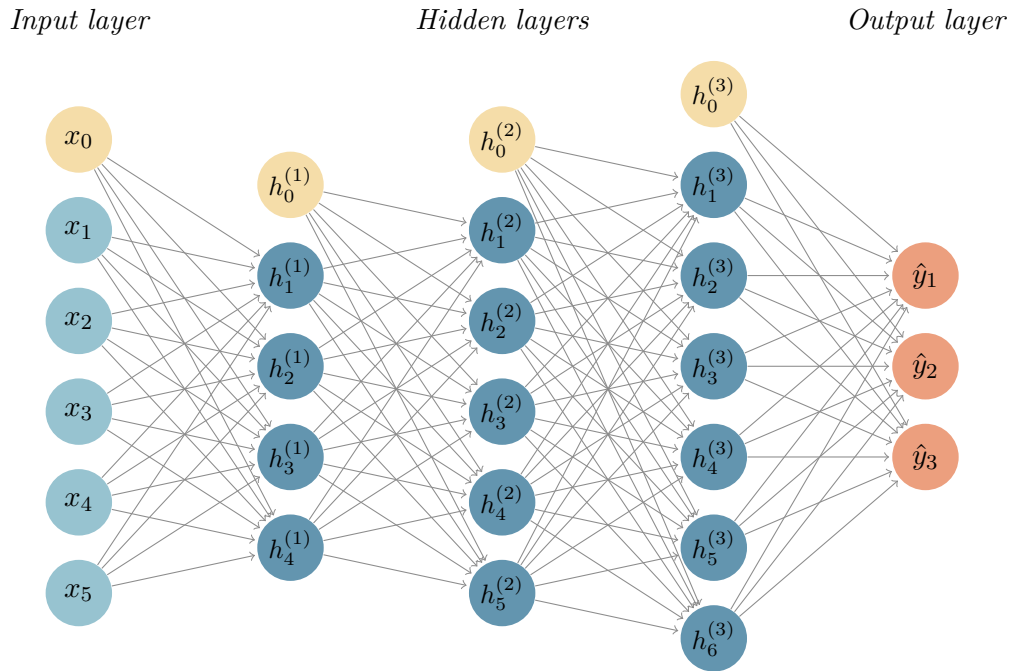


Figure S1: Example of a deep neural network with 3 hidden layers. The inputs (light blue nodes) are passed through the layers, with links between layers representing the weight matrices \mathbf{W} . Each layer also applies a *bias* (yellow nodes), with the network finally producing an output (orange).

Constructing the admittance matrix

Here we provide some additional information on the calculation of the network edge weights from the data. The weights quantify the admittance (inverse impedance) of the line, that is, how easily the line can transmit electrical current. The

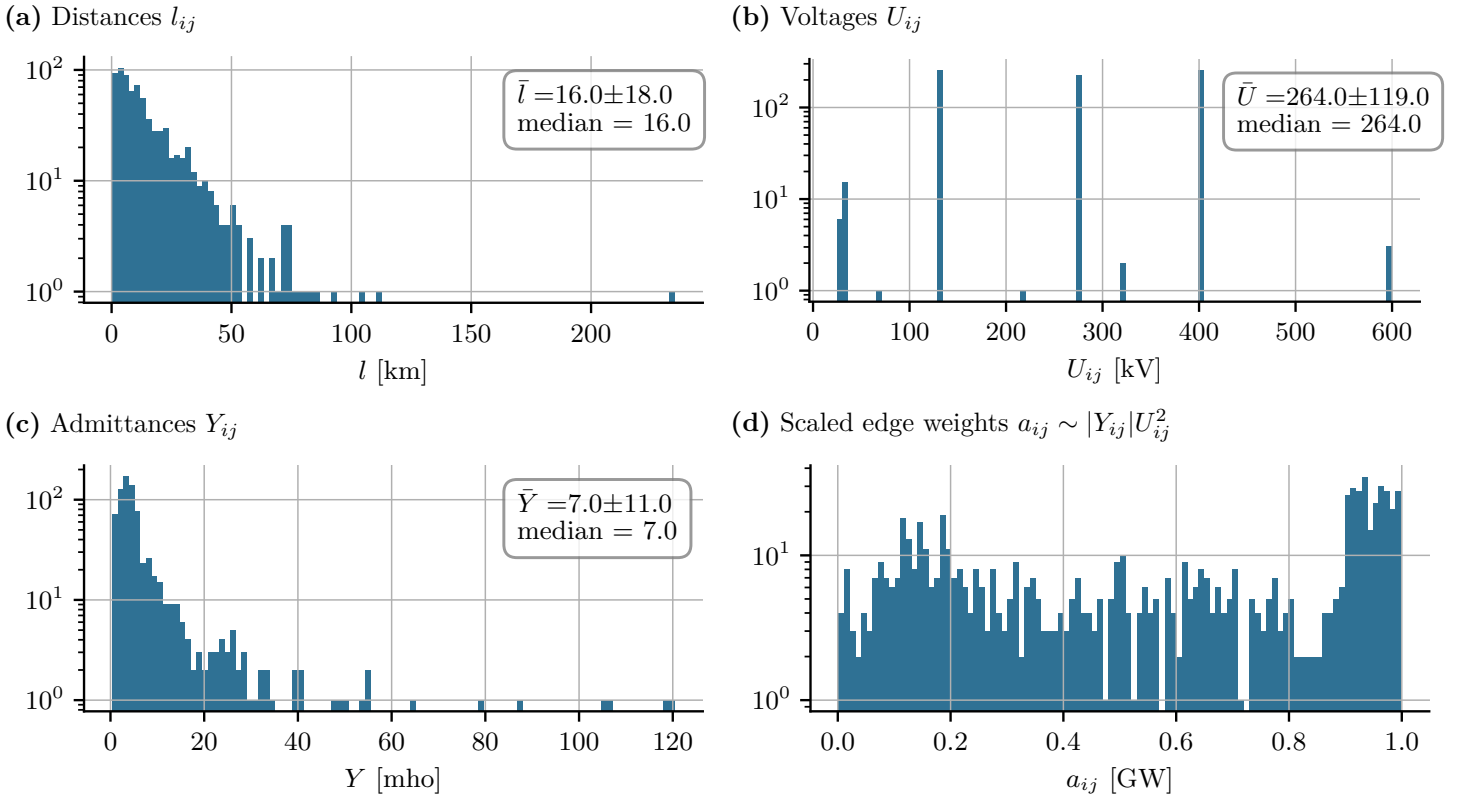


Figure S2: Line data statistics for the British power grid. (a) Histogram of the node distances in the network, with mean, standard deviation, and median given. (b) Histogram of the line voltages. (c) Histogram of the line admittances. As is visible, a small number of short lines artificially skew the distribution. (d) The resulting normalised edge weights. Short edges with an artificially high admittance are assigned a random value in $[0.9, 1]$.

characteristic impedance of a transmission line is given by

$$Z_0 = \sqrt{\frac{R + i\Omega L}{i\Omega C}}, \quad (11)$$

with i the complex unit, $\Omega = 50$ Hz the grid frequency [53], L the cable inductance, and C its capacitance. We use the following values for a copper conductor with a cross-section of 1000 mm², provided by a standard manufacturer⁴ of power grid cables: $R = 0.0276$ Ω /km (AC resistance), $L = 0.41$ mH/km, $C = 0.150$ μ F/km (assuming a single core). The total impedance along the line is then given by

$$Z(l) = Z_0 \sinh(\gamma l), \quad (12)$$

where l is the length of the line, and the propagation constant γ is given by

$$\gamma = \sqrt{(R + i\Omega L)(i\Omega C)}. \quad (13)$$

In these calculations we neglect the conductance of the dielectric along the line, which is negligible at the distances present in the network. The admittance of the line is then given by

$$Y_{ij} = Z_{ij}^{-1}, \quad (14)$$

and the total edge weight a_{ij} by

$$a_{ij} = |Y_{ij}|U_{ij}^2. \quad (15)$$

⁴caledonian-cables.co.uk/products/hv/400kv.shtml

Long lines typically carry two to four times as many cables as shorter lines. We account for this by multiplying the admittance of lines over 10 km by a factor of 2, and those over 80 with a factor of 3 (admittances are additive). Since the neural network outputs values in $[0, 1]$, we scale the edge weights to this range. However, a small number of short lines artificially skew the distribution (see figure S2); these are mainly small segments designed to more accurately capture the geometry of a longer line, though sometimes they represent short lines to transformers, power stations, etc. To reduce their impact on the weight distribution, instead of dividing the weights by the maximum value, we divide by the mean and truncate all weights to $[0, 1]$:

$$a_{ij} \rightarrow \min(1, a_{ij}/\langle a_{ij} \rangle). \quad (16)$$

The scaling factor is absorbed into the coupling coefficient κ . Those edges with weight exactly equal to 1 are reassigned a value chosen uniformly at random in $[0.9, 1.0]$. As is visible in fig. S2d, the resulting distribution of the weights a_{ij} is more uniform than that of the distances l_{ij} and admittances Y_{ij} , since longer lines' lower admittance is often compensated by a higher voltage.

These calculations do not account for, among other things, the fact that we are connecting the nodes with straight lines rather than the real line trajectory, are not discerning between overground and underground lines, are assuming a single core per cable, and are not considering differences in transmission line heights, geometries, and materials. These inaccuracies are absorbed into the coefficients α and β , which we tune manually in order to allow for stable phase-locking.

Details on the code

The code is uploaded to the [Github repository](#) as given in the main text. The two models relevant to this work are Kuramoto and HarrisWilsonNW.

Installation

Detailed installation instructions are given in the repository. First, clone the repository, install the [utopya](#) package and all the required additional components into a virtual environment, for example via PyPi. In particular, install [pytorch](#). Enter the virtual environment. Then, from within the project folder, register the project:

```
utopya projects register .
```

You should get a positive response from the utopya CLI and your project should appear in the project list when calling:

```
utopya projects ls
```

Note that any changes to the project info file need to be communicated to utopya by calling the registration command anew. You will then have to additionally pass the `--exists-action overwrite` flag, because a project of that name already exists. See

```
utopya projects register --help
```

for more information. Finally, register the project and its models via

```
utopya projects register . --with-models
```

Running the code

To run a model, execute the following command:

```
utopya run <model_name>
```

By default, this runs the model with the settings in the `<model_name>_cfg.yml` file. All data and the plots are written to an output directory, typically located in `~/utopya_output`. To run the model with different settings, create a `run_cfg.yml` file and pass it to the model like this:

```
utopya run <model_name> path/to/run_cfg.yml
```

This is recommended rather than changing the default settings, because the defaults are parameters that are known to work and you may wish to fall back on in the future.

Plots are generated using the plots specified in the `<model_name>_plots.yml` file. These too can be updated by creating a custom plot configuration, and running the model like this:

```
utopya run <model_name> path/to/run_cfg.yml --plots-cfg path/to/plot_cfg.yml
```

See the [Utopia tutorial](#) for more detailed instructions.

All the images in this article can be generated using so-called *configuration sets*, which are complete bundles of both run configurations and evaluation configurations. For example, to generate the predictions on the random network with $N = 1000$ nodes (fig. 6d-e) for the Kuramoto model, you can call

```
utopya run Kuramoto --cfg-set N_1000_example
```

This will run and evaluate the Kuramoto model with all the settings from the `Kuramoto/cfgs/N_1000_example/run.yml` and `eval.yml` configurations.

Parameter sweeps

Parameter sweeps are automatically parallelised by `utopya`, meaning simulation runs are always run concurrently whenever possible. The data is automatically stored and loaded into a data tree. To run a sweep, simply add a `!sweep` tag to the parameters you wish to sweep over, and specify the values, along with a default value to be used if no sweep is performed:

```
param: !sweep
  default: 0
  values: [0, 1, 2, 3]
```

Then in the run configuration, add the following entry:

```
perform_sweep: true
```

Alternatively, call the model with the flag `--run-mode sweep`. The configuration sets used in this work automatically run sweeps whenever needed, so no adjustment is needed to recreate the plots used in this work.

Initialising the neural net

The neural net is controlled from the `NeuralNet` entry of the configuration:

```
NeuralNet:
  num_layers: 4
  nodes_per_layer:
    default: 20
    layer_specific:
      1: 10
      2: 15
  biases: # optional; if this entry is omitted no biases are used
    default: ~ # default is None (indicted by a tilde in YAML)
    layer_specific:
      0: default # use pytorch default (xavier uniform)
      -1: [-1, 1] # uniform initialisation on a custom interval
  activation_funcs:
    default: sigmoid
    layer_specific: # optional
      1: tanh
```



```

3:
  name: HardTanh # you can also pass a function that takes additional args and/or kwargs
  args:
    - -2 # min_value
    - +2 # max_value
  learning_rate: 0.001 # optional; default is 0.001
  optimizer: SGD # optional; default is Adam

```

`num_layers` specifies the depth of the net; `nodes_per_layer` controls the architecture: provide a `default` size, and optionally any deviations from the default under `layer_specific`. The keys of the `layer_specific` entry should be indices of the layer in question. The optional `biases` entry determines whether or not biases are to be included in the architecture, and if so how to initialise them. A default and layer-specific values can again be passed. Setting an entry to `default` initialises the values using the pytorch default initialiser, a Xavier uniform initialisation. Passing a custom interval instead initialises the biases uniformly at random on that interval, and passing a tilde `~` (None in YAML) turns the bias off. `activation_funcs` is a dictionary specifying the activation functions on each layer, following the same logic as above. Any [pytorch activation function](#) is permissible. If a function requires additional arguments, these can be passed as in the example above. Lastly, the `optimizer` keyword takes any argument [allowed in pytorch](#). The default optimizer is the Adam optimizer [26] with a learning rate of 0.02.

The neural net can be initialised from different initial values in the parameter space by changing the *random seed* in the configuration:

```
seed: 42
```

Sweeping over different initialisations is achieved by sweeping over the seed, as described in the previous section.

Training the neural net

The `Training` entry of the configuration controls the training process:

```

Training:
  batch_size: 2
  device: cpu
  true_parameters:
    sigma: 0.0
  loss_function:
    name: MSELoss
    # can pass additional args and kwargs here ...

```

You must specify the noise level to use for the ABM during training; the default value is 0. Under the `loss_function` key you can specify the loss function to use, and pass any arguments or keyword arguments it may require using an `args` or `kwargs` key. You can use any available [pytorch loss function](#).

The `device` key sets the training device. The default is the CPU, but you can also train on the GPU by setting the device to `cuda`. Note that on Apple Silicon, the device name is `mps`. Make sure you have installed the correct package for your device, and note that, as of writing, some pytorch functions required for our code (e.g., the `trace` and `hard sigmoid` functions) had not yet been implemented for MPS, hence GPU training on Apple Silicon devices was not possible.

Kuramoto model

Neural Network Architecture

The following is the default configuration for the neural network and training settings used for the Kuramoto model:

```

Kuramoto:
  NeuralNet:

```

```

num_layers: 5
nodes_per_layer:
  default: 20
biases:
  default: ~ # No biases
activation_funcs:
  default: tanh
  layer_specific:
    -1: HardSigmoid # hard sigmoid on the last layer
learning_rate: 0.002
optimizer: Adam
Training:
  batch_size: 2
  loss_function:
    name: MSELoss
  true_parameters:
    sigma: 0

```

Training

We rewrite [4] as a vector-matrix equation,

$$\alpha \frac{d^2 \boldsymbol{\varphi}}{dt^2} + \beta \frac{d \boldsymbol{\varphi}}{dt} = \mathbf{P} + \kappa \text{diag}(\mathbf{A}\boldsymbol{\Gamma}(\boldsymbol{\varphi})),$$

which is more amenable to machine learning purposes, since it can make use of fast matrix-multiplication operations. $\mathbf{\Gamma}$ is the interaction kernel matrix, $\Gamma_{ij} = \sin(\varphi_j - \varphi_i)$. We train the model using the following numerical operation: let $\boldsymbol{\varphi}(t) = (\varphi_1(t), \dots, \varphi_N(t))$ be the current phases of the N nodes, $\dot{\boldsymbol{\varphi}}(t) = (\varphi_1(t) - \varphi_1(t-1), \dots, \varphi_N(t) - \varphi_N(t-1))$ the vector of phase derivatives, $\boldsymbol{\omega} = (\omega_1, \dots, \omega_N)$ the vector of eigenfrequencies, and $\boldsymbol{\Gamma}(t) = (\sin(\varphi_j(t) - \varphi_i(t)))_{ij}$; then in each iteration of the first-order Kuramoto model ($\beta \neq 0$), we do

$$\boldsymbol{\varphi}(t+1) = \boldsymbol{\varphi}(t) + \frac{1}{\beta} \left(\boldsymbol{\omega}(t) + \text{diag} \left(\hat{\mathbf{A}}\boldsymbol{\Gamma}(t) \right) \right) dt, \quad (17)$$

where $\text{diag}(\cdot)$ takes the diagonal elements of the matrix. For the second-order model ($\alpha \neq 0$), we do

$$\boldsymbol{\varphi}(t+1) = \boldsymbol{\varphi}(t) + \frac{1}{\alpha} \left[\left(\boldsymbol{\omega}(t) + \text{diag} \left(\hat{\mathbf{A}}\boldsymbol{\Gamma}(t) \right) - \beta \dot{\boldsymbol{\varphi}}(t) \right) dt + \dot{\boldsymbol{\varphi}}(t) \right] dt. \quad (18)$$

In the first-order case, the initial conditions required are $\boldsymbol{\varphi}(0)$, in the second order case, we need $\boldsymbol{\varphi}(0)$ and $\dot{\boldsymbol{\varphi}}(0)$ (i.e. the initial phases and initial velocities).

Running the code

Configuration sets to reproduce all numerical experiments except the British power grid inference are provided; for instance, to produce the predictions for a random network with $N = 100$ nodes, simply run

```
utopya_run Kuramoto --cfg-set N_1000_example
```

Harris-Wilson model

Neural Network Architecture

The following is the default configuration for the neural network and training settings used for the Harris-Wilson model:

```

HarrisWilsonNW:
  NeuralNet:
    num_layers: 2
    nodes_per_layer:
      default: 20
    biases:
      default: ~ # No biases
    activation_funcs:
      default: tanh
      layer_specific:
        -1: sigmoid # sigmoid on the last layer
    learning_rate: 0.002
    optimizer: Adam
  Training:
    batch_size: 2
    loss_function:
      name: MSELoss
    true_parameters:
      sigma: 0

```

Training

We use the following matrix form of the Harris-Wilson equations to train the neural net. Let $\mathbf{D} \in \mathbb{R}^M$, $\mathbf{O} \in \mathbb{R}^N$, $\mathbf{W} \in \mathbb{R}^M$ be the demand vector, origin zone size vector, and destination zone size vector respectively. The the dynamics are given by

$$\mathbf{D} = \mathbf{W}^\alpha \odot \left[(\mathbf{C}^\beta)^T (\mathbf{O} \odot \mathbf{Z}) \right] \in \mathbb{R}^M, \quad (19)$$

with \odot indicating the Hadamard product, and elementwise exponentiation. $\mathbf{Z} \in \mathbb{R}^N$ is the vector of normalisation constants

$$\mathbf{Z}^{-1} = \mathbf{C}^\beta \mathbf{W}^\alpha. \quad (20)$$

The dynamics then read

$$\dot{\mathbf{W}} = \mathbf{W} \odot \epsilon(\mathbf{D} - \kappa \mathbf{W}) \quad (21)$$

with given initial conditions $\mathbf{W}(t = 0) = \mathbf{W}_0$. This formulation is more conducive to machine learning purposes, since it contains easily differentiable matrix operations and does not use for-loop iteration.

Running the code

This is analogous to the Kuramoto case. To reproduce the plot from the main article, run the following command:

```

utopya run HarrisWilsonNW --cfg-set London_dataset

```